Peer-reviewed version available at Materials 2020, 13, 956; doi:10.3390/ma13040956

Article

Relationship between the size and inner structure of AM powder particles

Kateřina Opatová [1,*], Ivana Zetková [2] and Ludmila Kučerová[3]

[1] Regional Technological Institute, University of West Bohemia, Pilsen, Czech Republic; opatovak@rti.zcu.cz
[2] Regional Technological Institute, University of West Bohemia, Pilsen, Czech Republic; zetkova@rti.zcu.cz
[3] Regional Technological Institute, University of West Bohemia, Pilsen, Czech Republic; skal@rti.zcu.cz
* Correspondence: opatovak@rti.zcu.cz; Tel.: +420 775 743 328

Abstract: Additive manufacturing (AM) is today's buzzword – and not only in commercial production. One of the AM techniques produces 3D objects with complex geometry using a laser beam. The relationship between the morphology of individual powder particles and the printing process has not been adequately documented yet. This article presents a detailed microscopic analysis of virgin and reused powder particles of maraging steel. Metallographic observation was performed using a scanning electron microscope (SEM). Detailed analyses of individual particles were carried out using SEM with a focused ion beam (FIB) milling capability. Analyses of elemental distribution and phase distribution were performed using EDS and EBSD, respectively. The findings have led to a better understanding and prediction of defects in additive-manufactured products.

Keywords: additive manufacturing; FIB; EBSD; EDS; maraging steel

1. Introduction

With additive manufacturing technology (AM), it is possible to create high-quality intricate metal parts with a potential for use in the aerospace, automotive or medical industries. Unlike conventional metal manufacturing processes, where the material is removed in order to obtain the desired shape, additive manufacturing works on the principle of adding and sintering individual layers of material. In this way, it is possible to produce complex-shape parts which may contain a plurality of internal elements, such as cooling channels [1,2]. Only a minimum amount of material is scrapped during the production because the powder used for printing can be recycled and reused. This makes it possible to efficiently use up to 97% of the input material. [3].

In order to obtain the required properties, it is essential that the input material (in this study, it is a metal powder marketed as EOS MaragingSteel MS1) is of high quality and its properties are consistent and thoroughly-described across all batches. The particle size distribution significantly affects the quality of the resulting product. The product quality also depends on whether a new or reused powder is used. Generally speaking, if a superior-quality product is to be obtained, all batch-specific deficiencies should be identified. These may include the presence of non-spherical particles, crushed particles, inclusions or gas entrapped in the particles during their production, particles of inappropriate size, or poor overall size distribution of the powder in the batch. All these parameters are influenced by the method of production of the metal powder and its subsequent handling, not only during recycling but also during preparation for printing. [3–6].

1.1. Production of metal powder and its quality control

Metal powders are usually manufactured using either mechanical or chemical processes. The methods include water atomization, milling, mechanical alloying, electrolysis, and chemical

methods, including the reduction of oxides. The choice of a production process depends on the requirements for the powder, such as the desired amount and physical and chemical properties. Chemical and electrolytic methods are suitable for producing high-quality materials. Mechanical preparation, such as milling, is good for preparing high-hardness or oxide-based materials. Most powders used in AM are produced by atomization or milling. Both are extremely energy-consuming processes [7,8].

Atomization is probably the most widespread method, and has the broadest scope of use. The input material for this study was made by atomization. It involves molten metal being carried by a high-speed inert gas (nitrogen, argon, helium) through a disperser, which produces droplets that cool rapidly. The resulting spherical particles are collected in a container. The cooling rates range from 10^2 to 10^7 °C*s $^{-1}$. They lead to what is known today as rapid solidification (RS). The typical size of the particles is up to 150 μm, although larger particles are not unusual. Ideally, the particles obtained by gas atomization should be smooth and spherical. In practice, some include "satellites": smaller particles adhering to larger ones. The likely cause of this is that smaller particles swirl in the collecting container and collide with larger, partially-melted particles which just entered the container [3,5,7–9].

The production of metal powders involves a quality control step, which can rely on either a standard powder sieve analysis according to ASTM B214 or, as in this experiment, laser diffraction analysis [10]. The quality control process is significantly impaired by particles of irregular shapes, be it satellites or non-spherical particles.

1.1.1. Powder sieve analysis

Powder sieve analysis – as described in ASTM B214 standard – separates metal powder particles based on their size. Sieves with dry meshes are used which have various sizes of openings from 5 to 850 μm. The method provides very good repeatability but it does not yield information about the shape of individual particles. However, the knowledge of the size distribution is essential for obtaining high-quality AM products. The output from this measurement is volume fractions of particles in certain size intervals [11].

The principle of the method consists in stacking sieves of different mesh sizes on top of each other. The stack with a powder sample placed on top is then shaken (mostly by mechanical means), until the residues on each sieve contain only those particles that have fallen through the above sieve, but cannot pass through the underlying one. This method is too time-consuming for commercial environments. It is usually performed either during changeovers or periodically after certain time intervals [7].

1.1.2. Laser diffraction analysis

In contrast, laser diffraction analysis allows for real-time monitoring of particle size distribution during production and, at the same time, provides instant feedback for optimizing the production [3].

It is one of the most widely-used methods of measuring the particle size. It is working on the principle of coherent light scattering. Particles, while suspended in a slurry, pass in front of a laser beam. The particle size distribution is determined from the angle and intensity of the diffracted light. Today, laser diffraction can effectively measure particles within the size range of 0.01 μm to 5000 μm, which includes the entire size interval required for AM powder production. The output from this method is the same as that from the powder sieve analysis, i.e. volume fractions of particles from certain size intervals [7].

This method, either, cannot determine the shape of measured particles. However, this aspect is important for ensuring continuous flow of metal powder during the AM process. Determination of circularity of individual particles is time-consuming and is normally done manually using a microscope [3].

In order to identify differences between new and used powders, their samples were observed in a scanning electron microscope (SEM). All the above-mentioned defects were examined, which

adversely affect the quality of the resulting product (undesirable particle size distribution, out-of-roundness and internal defects in individual powder particles) [12].

2. Materials and Methods

The EOS MaragingSteel MS1 metal powder has been developed by EOS specifically for use with EOSINT M systems. Its chemical composition corresponds to the US grade 18% Ni Maraging 300, the European 1.2709 and the German X3NiCoMoTi 18-9-5 grades (Table 1). This steel is characterized by very good mechanical properties and heat treatability after printing. Its heat treatment sequence consists of stress-relieving and age hardening, which lead to high strength and hardness in the final product [13].

wt [%]	C	Si	Mn	P	S	Cr	Mo	Ni	Co	Ti	Cu	Al	Fe
MS 1	≤ 0.03	≤ 0.1	≤ 0.1	≤ 0.01	≤ 0.01	≤ 0.5	4.5 - 5.2	17.0 – 19.0	8.5 – 9.5	0.6 – 0.8	≤ 0.5	0.05 – 0.15	bal.

Table 1. Chemical composition of the experimental material, EOS MaragingSteel MS1 [13]

The particle size range reported by the manufacturer is between 10 µm and 63 µm, with the average of 50 µm (Figure 1). The particle size distribution was examined in this experiment.

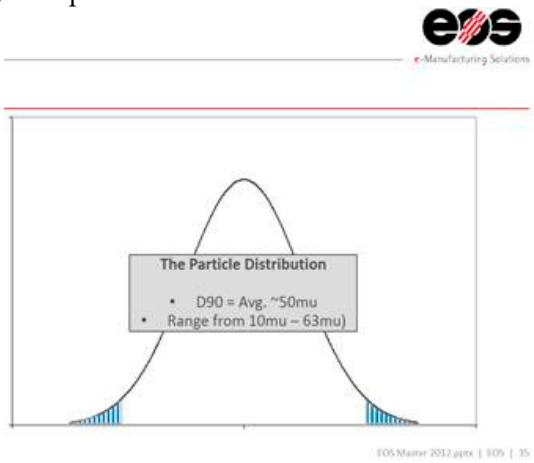

Figure 1. The particle distribution of EOS MaragingSteel MS1 - EOS. Training materials - Follow up training. Internal documentation

The measurement was performed in the scanning electron microscope Zeiss AURIGA fitted with the field emission gun of the Schottky type an a resolution of the electron beam of 1 nm. The system also featured a Focused Ion Beam (FIB) gun, detectors of secondary and back-scattered electrons (SE, BSE), an energy-dispersive X-ray spectroscopy (EDS) detector, electron backscatter diffraction (EBSD), and scanning transmission electron microscopy (STEM) capabilities for thin specimens.

Three types of specimens were prepared:

- virgin powder – taken from randomly-chosen locations in a newly open barrel of powder,
- reused powder – powder which passed through a sieve for recycling,
- residual oversize powder from the sieve after recycling.

All the specimens were mounted on SEM stubs on carbon adhesive discs. The diameters of metal powder particles were measured in the SmartTiffV3 software from Zeiss and in ImageJ software [14].

The size distribution and circularity of each powder type (virgin powder, reused powder and residual oversize powder) were measured. The surfaces of individual powder particles were examined (the surfaces of reused powder particles differ from the new powder, probably because of

differences in their formation processes). Some powder particles were then cut using FIB in order to examine their inner structure and defects, such as inclusions and chemical inhomogeneity. Approximately 30 virgin powder particles and 30 reused powder particles were cut. The parameters of milling were consistent, 100 nA current for coarse milling, 30 nA current for coarse polishing and 10–3 nA for fine polishing. With some particle sizes, lower current had to be used for final polishing (smaller particles of the virgin powder required lower current for polishing for microstructure analysis). Representative particles from several size categories were chosen for cutting and examination in order to gain comprehensive knowledge about the dependence of the inner morphology of particles on their size and manufacturing history. The cut surfaces were characterized using EDS and EBSD. For this purpose, a special holder for SEM stubs was used. The holder is pre-tilted at 54°, making it possible to cut the sample from one side and then perform EDS and EBSD analyses (Figure 2).

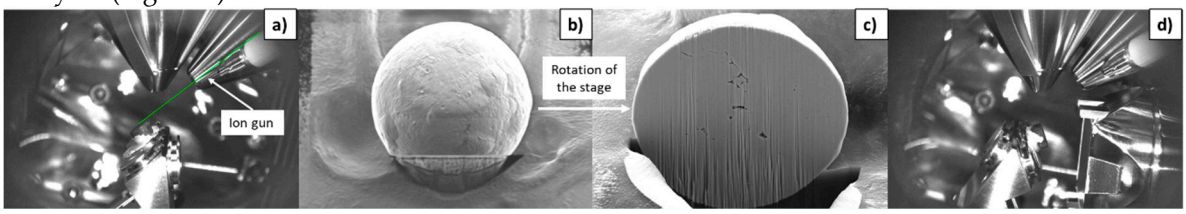

Figure 2. Sample preparation for EDS and EBSD analyses – a) ion milling and polishing, b) FIB image during milling, c) a sample in the position for EDS analysis, d) a sample in the position for EBSD analysis.

In this paper, band contrast images and inverse pole figure orientation maps from EBSD analysis are presented. Band contrast is an electron backscatter patterns (EBSP) quality factor derived from the Hough transform that describes the average intensity of the Kikuchi bands with respect to the overall intensity within the EBSP. These maps show the microstructure in a qualitative manner. Because EBSPs along grain boundaries tend to show poor band contrast, they appear dark in the map. Grain boundaries can thus be identified in undeformed structure. Inverse pole figure (IPF) orientation maps show the size, shape and orientation of grains in powder particles. Each individual orientation of crystals is colored differently. The color coding for orientations is presented in a Standard Stereographic Triangle (SST), which is inserted in IPF orientation maps. [15–17].

2. Results

2.1. Virgin powder

The particle sizes were measured in an electron microscope. It was found that the proportion of small particles (<10 μm) in the virgin powder sample is larger than that dictated by the size distribution reported by the supplier (Figure 3). The average particle size was a mere 25 μm. The measured average circularity was 0.93 (1 = perfectly circular particle). The measurement could be slightly different because of the different measurement method, but the fact that there is a larger number of small diameter particles in the sample than declared is obvious.

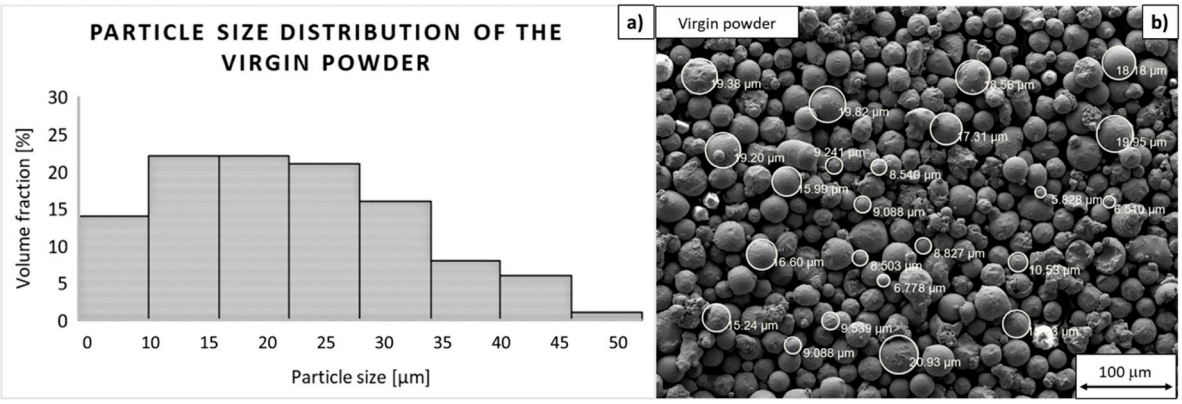

158

159 **Figure 3.** Virgin powder – a) particle size distribution, b) tentative particle size measurement in an
160 SEM image using SmartTiff software.

161 After their diameters had been measured, the particles were cut using focused ion beam.
162 Representative particles from each size category were randomly chosen for this analysis.
163 Micrographs taken using secondary electron imaging showed that there were some defects that
164 occurred mainly in particles of larger diameters. They were titanium segregations and cavities. For
165 better understanding and visualization of the defects, EDS and EBSD analyses were performed on
166 the cross-sections. Emphasis was placed on the shape of the defects and on the differences between
167 large and small particles. Cavities in the virgin powder were always spherical, with diameters up to
168 10 µm. Small cracks were found in the virgin powder, the dimensions of which did not exceed 5 µm.
169 In most cases, they were just located below the surface (Figure 4, 5).

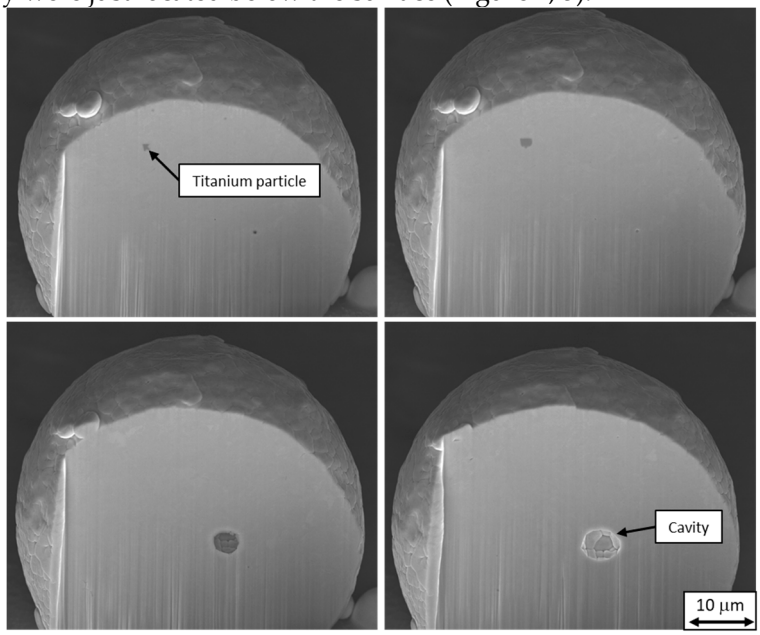

170

171 **Figure 4.** Images from FIB milling of a virgin powder particle with a sharp-edged titanium particle
172 and a cavity in the interior. Different shapes of these defects in successive cross-sections are shown in
173 the micrographs.

Peer-reviewed version available at Materials 2020, 13, 956; doi:10.3390/ma13040956

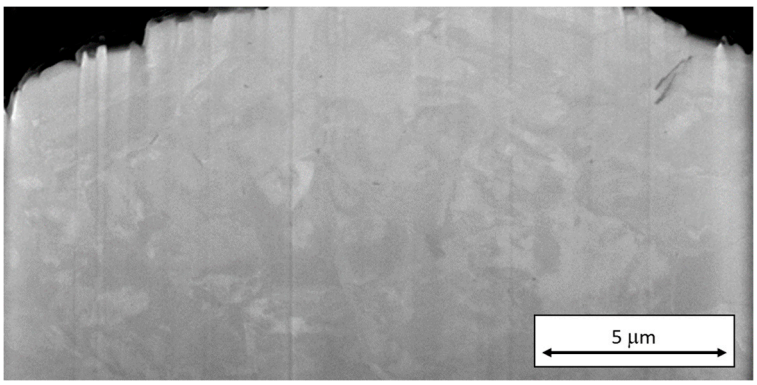

Figure 5. A crack below the surface of a virgin powder particle in an SEM micrograph taken during FIB milling. The inner structure of the particle has already been partially etched by the ion beam.

EDS analysis of the virgin powder revealed chemical segregation in its particles. This was more severe in particles of larger diameters (Figure 6 a). The most significant chemical heterogeneity is seen with titanium, iron and molybdenum (Figure 6 a, b). Titanium and molybdenum form closed cells in the structure of individual particles of every size. In larger particles, the internal structure is visible in secondary-electron images of surfaces after slight ion etching during FIB milling (Figure 6 a). This structure does not fully correspond to the distribution of chemical elements. However, the boundaries of structural units are sometimes delineated by segregated molybdenum.

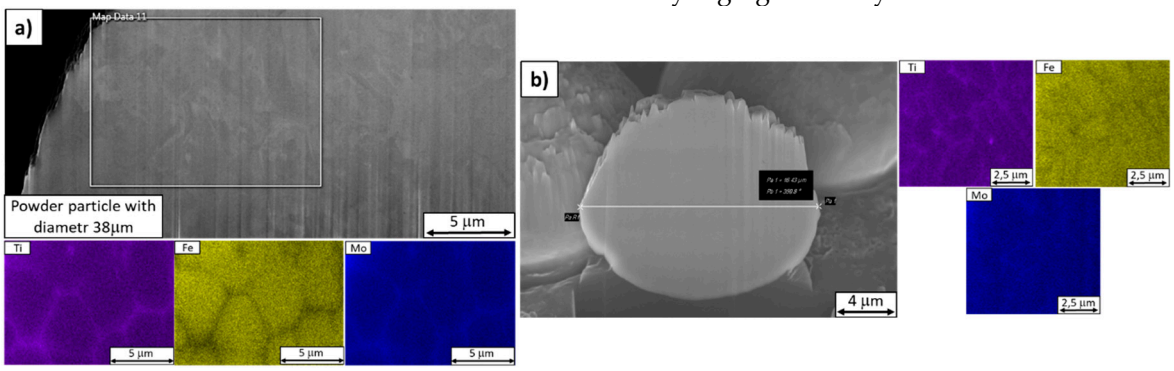

Figure 6. EDS analysis of the virgin powder – a) a larger particle with a diameter of 38 µm with a partially-etched microstructure, b) smaller particle, 16.5 µm in diameter.

EBSD analysis confirmed the internal particle structure which had been partially revealed by ion etching and viewed using secondary-electron imaging. It was found that segregated titanium and molybdenum occupied the boundaries of units of this inner structure. The size of these units in the virgin powder was from several hundred nanometers to several micrometers, as seen in the band contrast map (Figures 7, 8).

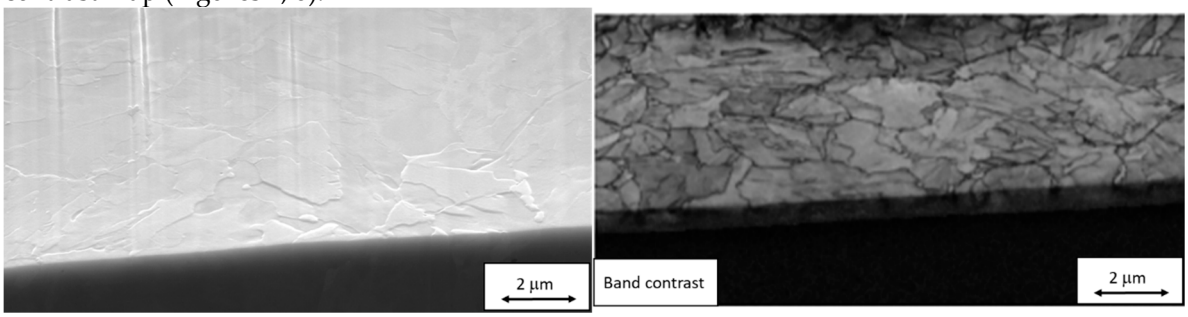

Figure 7. SEM micrograph of a virgin powder particle after ion-etching which revealed its inner structure; a band contrast map showing the boundaries of grains and sub-grains.

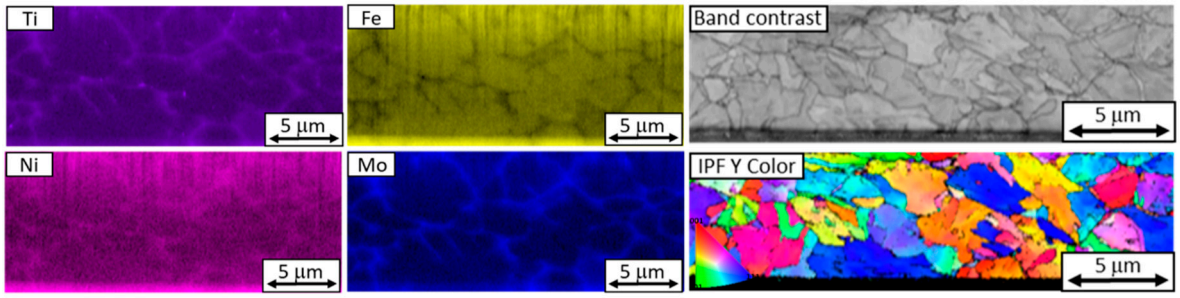

Figure 8. EDS and EBSD images of a virgin powder particle with chemical segregation along boundaries of its cellular structure. A band contrast map and an IPF map reveal the grain structure of the particle.

2.2. Reused powder

In the sample of the reused powder, newly-formed particles account for only a small fraction of its volume. There are differences between these newly-formed particles and the original particles from the virgin powder in terms of the surface appearance, size, circularity and inner defects. The newly-formed particles can be several times larger than the virgin powder particles, as they cool more slowly upon formation. These newly-formed particles were the focus of the analysis of the reused powder.

Measurements of the particle size distribution and circularity showed a much higher proportion of small particles (diameter < 10 µm) in the reused powder than in the virgin powder. It is probably caused by the difference between the conditions of creation of new particles during the printing process and those during atomization. The average size of reused powder particles was only 23 µm. The average circularity was 0.91 (Figure 9).

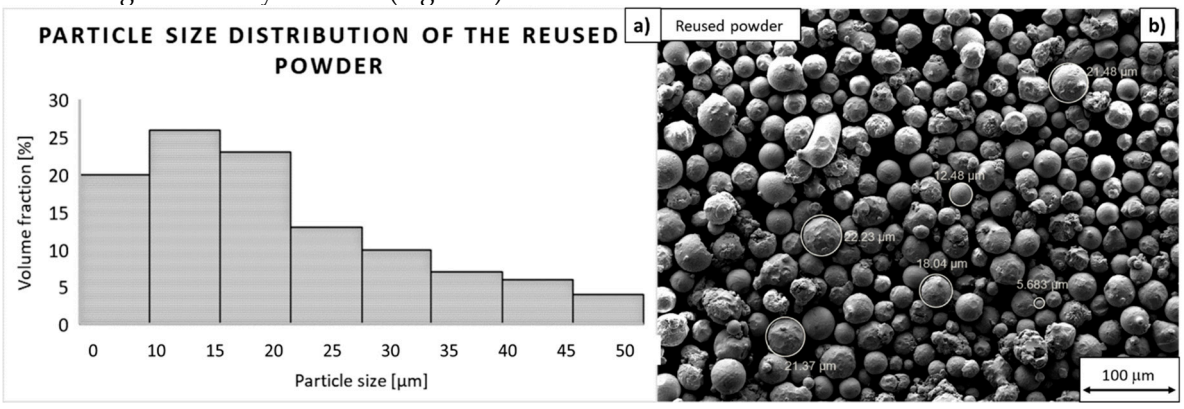

Figure 9. Reused powder - a) particle size distribution, b) tentative particle size measurement in an SEM micrograph using the SmartTiff software.

Reused powder particles are more distorted and more often non-round. The cavities in them are no longer strictly spherical, instead they have various elongated shapes, as revealed by FIB milling (Figure 10).

Peer-reviewed version available at Materials 2020, 13, 956; doi:10.3390/ma13040956

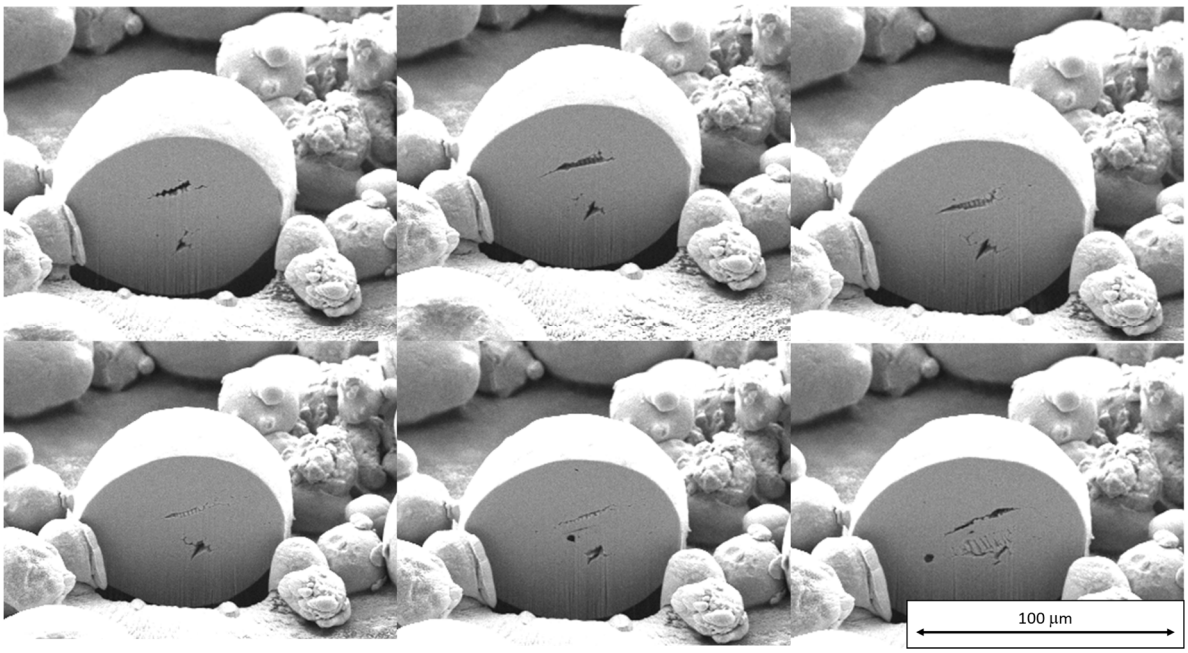

Figure 10. SEM images taken during FIB milling of a reused powder particle. Sections through the defects in the particle are shown. The shapes of these defects in the reused powder are not strictly spherical, in contrast to the virgin powder.

It was found that all reused powder particles of about 40 µm or more in size were certain to contain cavities. Cavities can also occur in smaller particles. The reused powder showed significant segregation of titanium as well. In contrast to the virgin powder, the reused powder particles contained globular titanium inclusions (Figure 11).

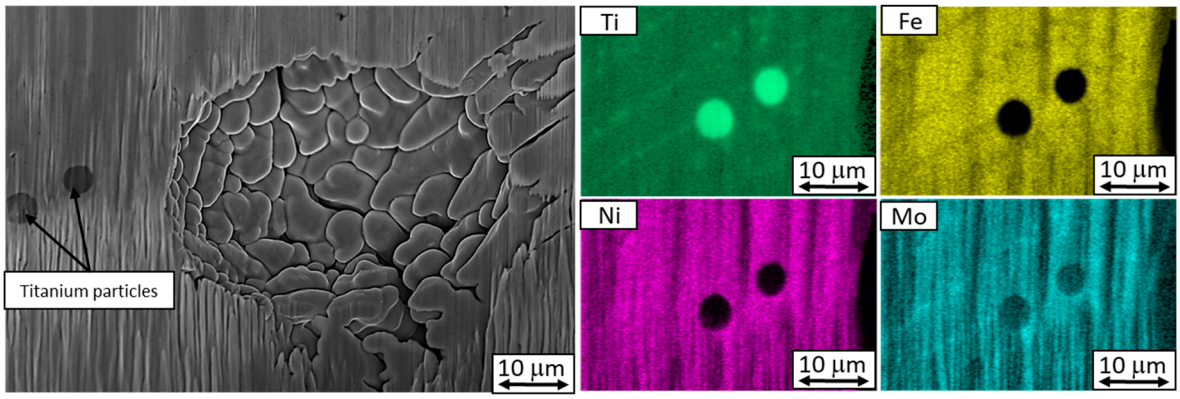

Figure 11. SEM image of an inclusion and titanium particles in a reused powder particle. Cracks can be seen along the boundaries of dendrites. The titanium particles in the reused powder are more circular than in the virgin powder.

The internal structure of reused powder particles consists of units delineated primarily by molybdenum, and also by titanium and nickel. These are larger than the units in the virgin powder particles (up to 10 µm), as shown in the band contrast micrograph (Figure 12).

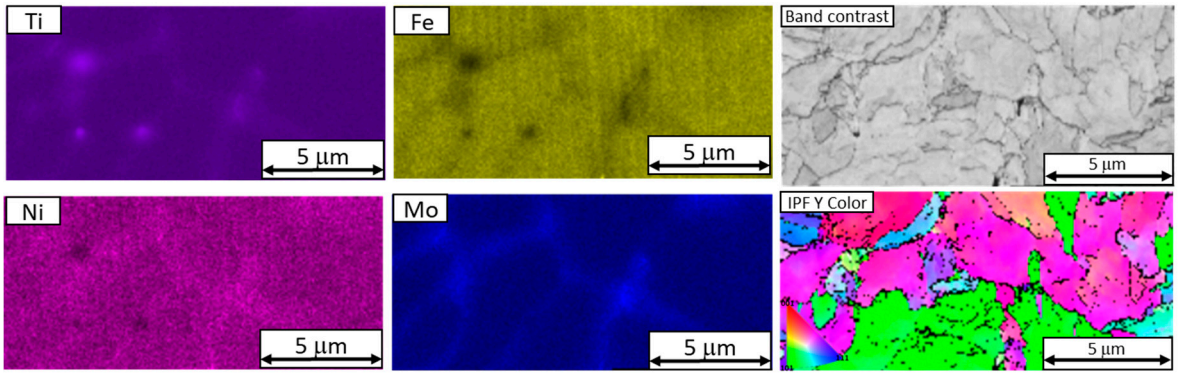

Figure 12. EDS and EBSD analysis of a reused powder particle with chemical segregation along the boundaries of the cellular structure. A band contrast map and an IPF map show the grain structure.

Chemical heterogeneity was observed in the surface of the particles which were newly-formed during printing. The chemical segregation, probably caused by slower cooling of these particles upon formation, was reflected in their different surface morphology. Two types of layers were found on their surface:

- titanium layers
- layers of titanium, molybdenum and nickel

These layers can lead to defects in printed products because they are difficult to melt. They form as a result of different densities of these chemical elements. The density of titanium is almost half that of the other elements in this material. Yet, its melting point is much higher than the melting point of the experimental material. The experimental material in the initial state can melt more readily than after its chemical constituents had been separated (in the form of layers on newly-formed particles).

In both reused and virgin powders, there was significant chemical segregation in their structure, namely with respect to titanium, molybdenum and nickel. In both powders, the boundaries of microstructure units were delineated by molybdenum. Their size ranged from hundreds of nanometers to several micrometers. In the reused powder, they were larger (Figure 13).

Peer-reviewed version available at Materials 2020, 13, 956; doi:10.3390/ma13040956

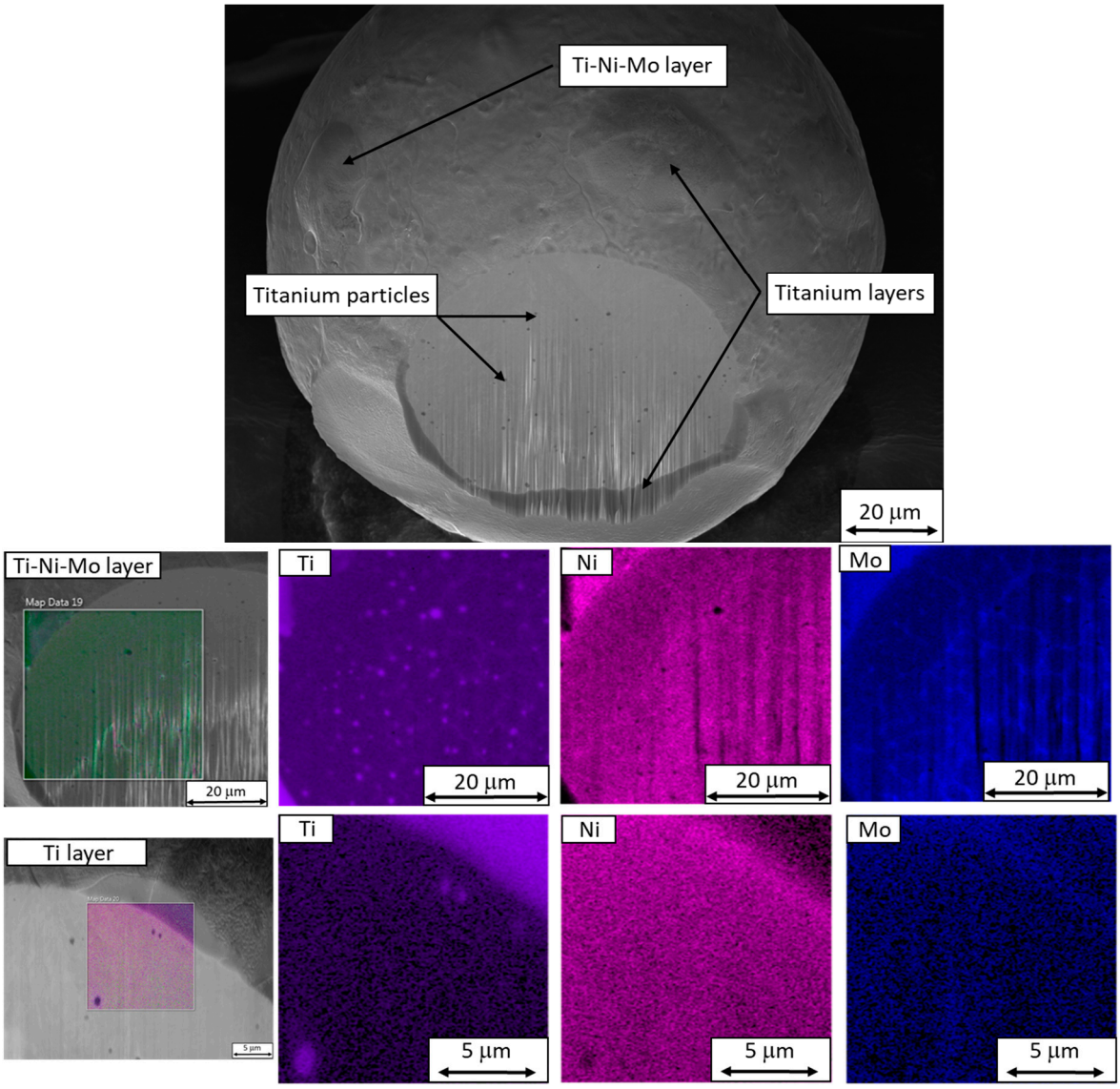

Figure 13. EDS analysis of a reused powder particle with differences between the Ti-layer and the Ti-Ni-Mo layer. Titanium particles and molybdenum segregation along the cellular structure can be seen.

2.3. Residual oversize powder from the sieve

On this sample, only the particle size distribution and circularity were measured. The reason was that this powder would not be used for building any more. The size distribution shows a drop in the amount of particles sized between 20 µm and 60 µm, as most of those were recycled for reuse.

The average particle size of the residual oversize powder after sieving was 58 µm, and the average circularity was just 0.88. Many satellites were found in the sample, as well as particles with surface layers of segregated titanium, nickel and molybdenum (Figure 14).

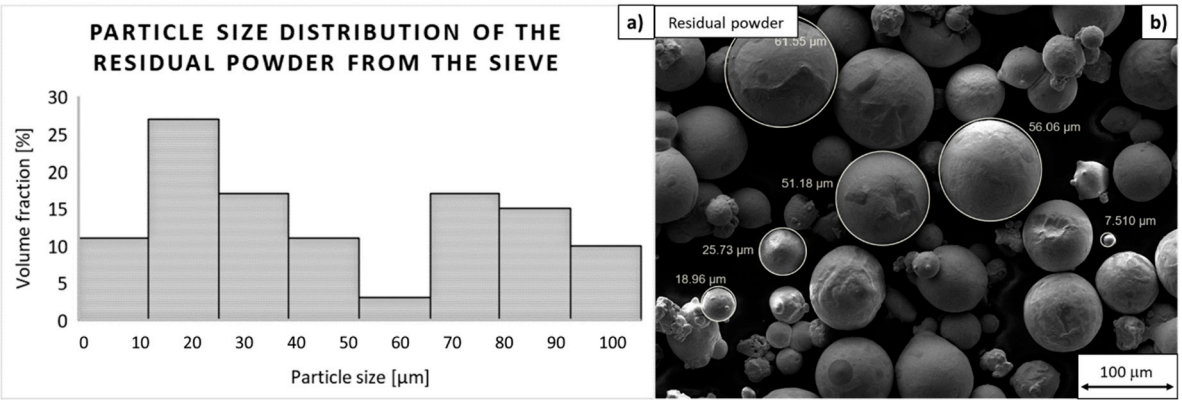

Figure 14. Residual oversize powder from the sieve - a) particle size distribution, b) tentative particle size measurement in an SEM image using the SmartTiff software.

3. Discussion

Given that the production of AM metal powders will exceed $500 million in 2019 and as much as $900 million worth in 2023 (40% annual growth), it is essential to be able to characterize the properties of these powders. The aim is to predict the quality of printed products and achieve savings in their production. Knowing the dependence of the behavior of metal powders on their particle shape, defects and size distribution can lead to optimized powder production and defect-free products [4].

In this paper, defects in metal powder particles were observed, such as internal inclusions, non-spherical shape and chemical heterogeneity. Differences between these defects in the virgin powder, reused powder and residual oversize powder from the recycling sieve were described. An electron microscope with a focused ion beam capability was used for analysis. EDS and EBSD examination was performed on individual particles. Measurement of particle size distribution revealed a major difference between the average particle size declared by the supplier (50 µm) and the measured one (25 µm).

The share of powder particles with internal defects in the form of cavities increases proportionately to the particle size. Newly-formed particles contained more cavities of this kind, possibly due to their formation mechanism being different from gas atomization [5]. By examining sufficient numbers of powder particles (approximately 30 virgin powder particles and 30 reused powder particles), it was found that no cavities were present in particles whose diameter was under 30 µm.

Chemical segregation on the surfaces of some reused particles can cause significant problems during their reuse for printing of metal products. Titanium exhibits the strongest tendency to form envelopes around newly-formed particles and its density is almost two times lower than that of the other chemical elements in this material. These particles will thus be likely to remain close to one another during handling and be used in a single moment and location during printing of the desired part. Shaking of the batch of metal powder during refilling of the printing chamber can cause lighter particles with titanium to raise to the top of the bed. Their higher melting point can lead to defects in the final printed part. The formation of such layers will be the subject of further investigation, because despite the small amount of titanium in this material (less than 1 wt %), there is a tendency for titanium particles to form. Moreover, the amount of titanium in these particles is more than two times higher than in the rest of the experimental material (more than 2 wt %).

In follow-up studies, the number of recycling cycles should be taken into account. In this study, a powder after a single recycling step was examined. With more recycling cycles, other particle defects may occur: non-spherical newly-formed particles, satellites or internal inclusions. These are associated with the significantly different process of formation of new particles during printing. It should therefore be examined in greater detail, namely in terms of the temperature and speed of formation.

The relationship between EDS and EBSD analysis of the particle structure should also be investigated in future work. Segregation of molybdenum was found to correspond with the boundaries of dendrites in the material. EBSD band contrast maps reveal the martensitic structure of the material. The powder particles therefore exhibit a type of microstructure similar to the printed material, in which dendrite boundaries and substructure within martensite can be revealed by various etching techniques [18].

Author Contributions: conceptualization, K.O.; methodology, K.O.; validation, K.O., I.Z. and L.K.; formal analysis, K.O.; investigation, K.O., I.Z., L.K.; resources, K.O.; data curation, K.O.; writing—original draft preparation, K.O.; writing—review and editing, I.Z., L.K.; supervision, L.K.; project administration, I.Z.; funding acquisition, I.Z.

Funding: This research was funded by the Technology Agency of the Czech Republic under the project TJ01000161 'Systematic applied research of material properties of martensitic steel W-Nr. 1.2709 produced by 3D printing using DMLS technology with the application of researchresults in practice'.

Conflicts of Interest: The authors declare no conflict of interest.

References

1. Attaran, M. The rise of 3-D printing: The advantages of additive manufacturing over traditional manufacturing. *Bus. Horiz.* **2017**, *60*, 677–688, doi:10.1016/j.bushor.2017.05.011.

2. Eyers, D. R.; Potter, A. T. Industrial Additive Manufacturing: A manufacturing systems perspective. *Comput. Ind.* **2017**, *92–93*, 208–218, doi:10.1016/j.compind.2017.08.002.

3. Levoguer, C. Using laser diffraction to measure particle size and distribution. *Met. Powder Rep.* **2013**, *68*, 15–18, doi:10.1016/S0026-0657(13)70090-0.

4. Thomas, M.; Drawin, S. Role of Metal Powder Characteristics in Additive Manufacturing. In *PM2016 world congress*; Hambourg, 2016.

5. J. S. DUNNING, R. C. D. M icrostructural characteristics and gas content of rapidly solidified powders. *J. Mater. Sci.* **1994**, *29*, 4268–4272.

6. Materials, O. F. Undercooling during atomization of V M300 maraging steel. *J. Mater. Sci.* **1974**, *9*, 1040–1043.

7. Lewandowski, C. M. Powder Metal Technologies and Applications. *ASM Int. Mater. Park. OH* **2015**, *7*, 2762, doi:10.1017/CBO9781107415324.004.

8. Achelis, L.; Uhlenwinkel, V. Characterisation of metal powders generated by a pressure-gas-atomiser. *Mater. Sci. Eng. A* **2008**, *477*, 15–20, doi:10.1016/j.msea.2007.07.095.

9. Anderson, I.E., White, E.M.H., Tiarks, J.A., Riedemann, T., Byrd, D.J., Anderson, R.D., Regele, J. D. Fundamental progress toward increased powder yields from gas atomization for additive manufacturing. In *Advances in Powder Metallurgy and Particulate Materials*; 2017; pp. 138–146.

10. J. A. Slotwinski, E. J. Garboczi, P. E. Stutzman, C. F. Ferraris, S. S. Watson, and M. A. P. Characterization of Metal Powders Used for Additive Manufacturing. *J. Res. Natl. Inst. Stand.*

Technol. **2014**, *119*, 460–493, doi:10.6028/jres.119.018.

11. ASTM International ASTM B214 - 16 Standard Test Method for Sieve Analysis of Metal Powders 2016.

12. Desai, P. S.; Mehta, A.; Dougherty, P. S. M.; Fred Higgs, C. A rheometry based calibration of a first-order DEM model to generate virtual avatars of metal Additive Manufacturing (AM) powders. *Powder Technol.* **2018**, *342*, 441–456, doi:10.1016/j.powtec.2018.09.047.

13. EOS GmbH Material Data Sheet - 18Ni300. **2011**, *49*, 6.

14. Rasband, W. S. ImageJ 2012.

15. Maitland, T.; Sitzman, S. EBSD Technique and Materials Characterization. *Scanning Microsc. Nanotechnology. Tech. Appl.* **2007**, 41–76.

16. Mutua, J.; Nakata, S.; Onda, T.; Chen, Z. C. Optimization of selective laser melting parameters and influence of post heat treatment on microstructure and mechanical properties of maraging steel. *Mater. Des.* **2018**, *139*, 486–497, doi:10.1016/j.matdes.2017.11.042.

17. Stojakovic, D. Electron backscatter diffraction in materials characterization. *Process. Appl. Ceram.* **2012**, *6*, 1–13, doi:10.2298/PAC1201001S.

18. Tan, C.; Zhou, K.; Ma, W.; Zhang, P.; Liu, M.; Kuang, T. Microstructural evolution, nanoprecipitation behavior and mechanical properties of selective laser melted high-performance grade 300 maraging steel. *Mater. Des.* **2017**, *134*, 23–34, doi:10.1016/j.matdes.2017.08.026.